

Numerical continuation in classical mechanics and thermodynamics

Aleix Gimenez¹, Victor Chausse¹ and Alvaro Meseguer²

¹ Escola Tècnica Superior d'Enginyeria de Telecomunicació de Barcelona (ETSETB)
Universitat Politècnica de Catalunya Edifici B3-Ricardo Valle Campus Nord Jordi
Girona, E-1-3 08034 Barcelona, Spain

² Department of Applied Physics, Universitat Politècnica de Catalunya B5 Campus
Nord Jordi Girona, E-1-3 08034 Barcelona, Spain

E-mail: alvaro.meseguer@upc.edu

Received 25 April 2014, revised 11 September 2014

Accepted for publication 3 October 2014


Published 24 November 2014



CrossMark

Abstract

In this paper, modern numerical continuation methodologies are presented as a way of understanding and computing multiplicity of solutions in undergraduate physics problems. Mechanical and thermodynamical problems are used as a storyline to introduce the mathematical formalism required to clarify the distinction between the uniqueness and multiplicity of equilibrium solutions and the critical states of a nonlinear physical problem, as well as to illustrate how these novel numerical continuation techniques are implemented in practice. The paper provides simple numerical MATLAB codes that are easily adaptable to other problems, as well as updated software and literature resources.

 Online supplementary data available from stacks.iop.org/ejp/36/015015/mmedia

Keywords: numerical methods, nonlinear systems, arclength continuation

1. Introduction

Numerical continuation methods are very powerful tools for understanding the concepts of multiplicity or nonuniqueness of solutions in nonlinear physics [1]. In academic physics courses, it is not always sufficiently emphasized that, for a prescribed set of external conditions, a given nonlinear physical problem may exhibit multiple solutions such as *equilibria* or *critical states*. Over the last four or five decades, nonlinearity in the physics literature has become the rule, not the exception. Concepts such as *chaos* and *bifurcation points* (sometimes also called *tipping points*) have progressively appeared more frequently. Whereas chaos and

bifurcation theory have already reached their maturity [2] as new branches of mathematical physics, their inclusion in undergraduate academic books is still in its early stage, since they are generally relegated to noncompulsory material and are always addressed from a qualitative point of view. One of the reasons for the limited scope of nonlinear problems in undergraduate syllabi is the average student's lack of a basic numerical analysis background. Nonlinearity and chaos are frequently introduced to undergraduates by means of simple, low-dimensional dynamical systems such as double pendulums or logistic maps [3–5]. From a pedagogical point of view, these types of physical models contain the essential ingredients for visualizing chaotic dynamics, requiring only very basic mathematical and numerical methodologies to formulate and approximate them, respectively. However, the analysis of the aforementioned problems frequently focuses on their dynamical aspects rather than on the underlying topological structure of the state space, which is characterized by the equilibrium solutions or critical points.

Bifurcations (i.e., topological changes in parameter-dependent phase spaces) lie at the very heart of chaotic dynamics. In nonlinear systems, this type of dynamics requires multiplicity of equilibria. When studying a nonlinear system, one must first explore the families of fixed points or critical solutions when parameters are varied. Numerical continuation methods are designed precisely for the purpose of tracking families of solutions of the nonlinear system as a function of some parameter, as well as monitoring their analyticity properties. The concept of parameter-dependent solutions can be extended to general nonlinear systems of algebraic equations in many branches of physics, ranging from optics and chemical kinetics to fluid dynamics.

A proper understanding of the concept of nonuniqueness of solutions in classical and modern physics requires new analytical and numerical approaches, not only to shed light on the underlying mechanisms responsible for the emergence of multiple solutions in nonlinear problems, but also to accurately predict their presence in parameter-dependent systems. From the theoretical point of view, the implicit function theorem (IFT) plays a crucial role in the required conditions that may give rise to the presence or absence of solutions. In academic environments, the enormous implications of the IFT regarding the existence and uniqueness of solutions in mathematical physics problems are not always properly stressed.

There are many excellent monographs on continuation methods available in the literature. However, these texts are usually intended for a more advanced audience, ranging from graduate students to specialized researchers. In this work, we attempt to introduce the undergraduate student to the concepts of algebraic nonlinearity and parametric dependence from mathematical and numerical points of view by using a more academic style. The analysis presented here pursues rigorous and detailed formulation of the mathematical problem, combined with the application of highly accurate, state-of-the-art numerical continuation methodologies. Although the techniques shown here are applicable to systems arising in many branches of nonlinear physics, we focus on academic problems in mechanics (the double rotating pendulum) and thermodynamics (study of phase transitions of real gases), which students should already be familiar with. The problems have been chosen for the sake of clarity, not for their particular complexity, thus allowing a straightforward mathematical formulation, as well as accurate and computationally efficient numerical implementation. With the two examples shown, we aim to illustrate how nonlinearity appears in many branches of physics and how a deep mathematical understanding of the nonlinear algebraic problem at hand can be addressed with universal methodologies.

Other mechanical problems, such as the stability of fluid flows or elastic media, could have been treated using numerical continuation methods [6]. However, addressing these problems would require that students have a strong mathematical background in the theory of

partial differential equations and numerical linear algebra. These topics are typically taught at a graduate or master level and are out of the scope of undergraduate audiences.

The paper is structured as follows. Section 2 is devoted to the mathematical and numerical formulation of continuation problems. This section also illustrates some of the concepts with a mechanical example that can be addressed analytically. Section 3 applies the numerical algorithms to a mechanical problem similar to the one analysed in section 2, but where numerical methods are needed; section 4 applies the same techniques within the framework of undergraduate thermodynamics. Finally, appendix A outlines the MATLAB codes used to solve the aforementioned problems.

2. Mathematical and numerical formulation

The mathematical formulation that leads to the determination of equilibrium or critical solutions of parameter-dependent physical problems generally boils down to systems of nonlinear equations. These equations may have an algebraically explicit expression, but in some cases, as we will see later, it is not always possible to write these equations in closed form. In any case, we consider a system of n nonlinear equations with n variables, $\mathbf{x} = (x_1, x_2, \dots, x_n)$, and one parameter³, α :

$$\begin{aligned} F_1(x_1, x_2, \dots, x_n, \alpha) &= 0 \\ F_2(x_1, x_2, \dots, x_n, \alpha) &= 0 \\ &\vdots \\ F_n(x_1, x_2, \dots, x_n, \alpha) &= 0. \end{aligned} \quad (1)$$

In a more compact fashion, the system of equations above can be written as $\mathbf{F}(\mathbf{x}, \alpha) = 0$, with $\mathbf{x} \in \mathbb{R}^n$, $\alpha \in \mathbb{R}$ and $\mathbf{F}: \mathbb{R}^{n+1} \rightarrow \mathbb{R}^n$. We can think of \mathbf{x} as the set of physical variables that describes a certain state of the system (position coordinates, angles, current intensities in a circuit, thermodynamic pressure or volume of a gas in equilibrium, etc), whereas α plays the role of an external forcing or condition that acts on the system, such as an oscillatory frequency imposed by a signal generator, an environmental temperature, etc.

Assume that, for some prescribed value of the external parameter, $\alpha = \alpha^0$, our physical system exhibits an equilibrium state, $\mathbf{x}^0 = (x_1^0, x_2^0, \dots, x_n^0)$. That is, $(\mathbf{x}^0, \alpha^0) = (x_1^0, x_2^0, \dots, x_n^0, \alpha^0)$ satisfies the system of equations (1). A natural question is how this solution changes under small variations of the parameter α (i.e., whether there are nearby qualitatively similar solutions, $\mathbf{x} = \mathbf{x}^0 + \Delta\mathbf{x}$, when the parameter is slightly changed to $\alpha = \alpha^0 + \Delta\alpha$, with $|\Delta\alpha|$ small). The answer to this question is provided by the IFT, which states that for those nearby solutions to exist, a necessary condition is for the *Jacobian* of \mathbf{F} at (\mathbf{x}^0, α^0) to be a nonsingular matrix [7]:

$$\begin{vmatrix} \partial_{x_1} F_1 & \partial_{x_2} F_1 & \cdots & \partial_{x_n} F_1 \\ \partial_{x_1} F_2 & \partial_{x_2} F_2 & \cdots & \partial_{x_n} F_2 \\ \vdots & \vdots & \ddots & \vdots \\ \partial_{x_1} F_n & \partial_{x_2} F_n & \cdots & \partial_{x_n} F_n \end{vmatrix}_{(\mathbf{x}^0, \alpha^0)} \neq 0. \quad (2)$$

If condition (2) is satisfied, the IFT guarantees the existence of a *unique* local map, $\mathbf{x} = \mathbf{x}(\alpha)$, in a neighbourhood of (\mathbf{x}^0, α^0) , satisfying $\mathbf{x}(\alpha^0) = \mathbf{x}^0$. In that case, it is said that system (1)

³ Although we make a clear distinction between the physical variables and the parameter, this categorization will be irrelevant later, when formulating continuation schemes.

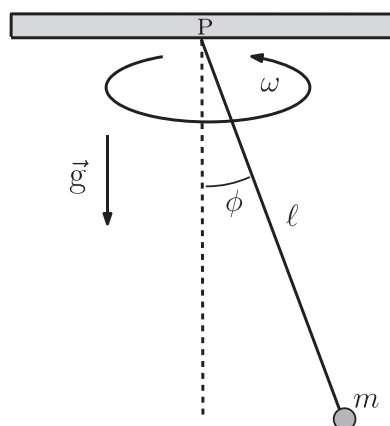


Figure 1. Rotating pendulum.

locally defines \mathbf{x} as a *unique implicit function*, $\mathbf{x}(\alpha)$, in a neighbourhood of the parameter value, $\alpha = \alpha^0$.

2.1. Nonuniqueness of equilibrium solutions: an analytical example

We illustrate some of the concepts previously seen by means of the academic problem of the rotating pendulum. Consider a pendulum consisting of a small marble of mass m , attached to a massless rigid rod of length ℓ . The rod–marble system is suspended under the effects of gravity from a fixed point, P , and is forced to rotate with a constant angular speed, $\omega > 0$, around a vertical axis passing through P (see figure 1). The purpose of this problem is to find the equilibrium angle, ϕ , such that the pendulum remains stationary in a frame rotating with angular speed ω . The equilibrium conditions are reduced to the system of nonlinear equations involving T (the rod's tension) and ϕ (the equilibrium angle):

$$\left. \begin{aligned} T \cos \phi &= mg \\ T \sin \phi &= m\ell\omega^2 \sin \phi \end{aligned} \right\}. \quad (3)$$

Therefore, the original system (3) is formally written as

$$\left. \begin{aligned} F_1(T, \phi, \omega) &= 0 \\ F_2(T, \phi, \omega) &= 0 \end{aligned} \right\}, \quad \text{with} \quad \left. \begin{aligned} F_1(T, \phi, \omega) &= T \cos \phi - mg \\ F_2(T, \phi, \omega) &= \sin \phi (T - m\ell\omega^2) \end{aligned} \right\}. \quad (4)$$

The question is whether the system (4) defines explicitly T and ϕ as unique functions of the external forcing, ω . System (4) offers two different families of solution branches:

- Solution branch (i): $(T, \phi, \omega) = (mg, 0, \omega)$, valid for all $\omega > 0$.
- Solution branch (ii): $(T, \phi, \omega) = (m\ell\omega^2, \arccos(g/\ell\omega^2), \omega)$, valid for all $\omega \geq \left(\frac{g}{\ell}\right)^{1/2}$.

Figure 2 shows the two families of equilibrium solutions parametrized as a function of the angular speed, ω . For $\omega < \omega_c$, the only available equilibrium solution is branch i: $(\phi_I, T_I) = (0, mg)$. Branch ii is born at a critical frequency, $\omega_c = (g/\ell)^{1/2}$. Beyond ω_c , three equilibrium solutions coexist for the same frequency: $\phi_I(\omega)$, $\phi_{II}(\omega)$, and its symmetric counterpart, $-\phi_{II}(\omega)$, due to the reflection symmetry of the problem. At $\omega = \omega_c$, the uniqueness of solutions is lost, and this can be identified *a priori* by testing the full-rank

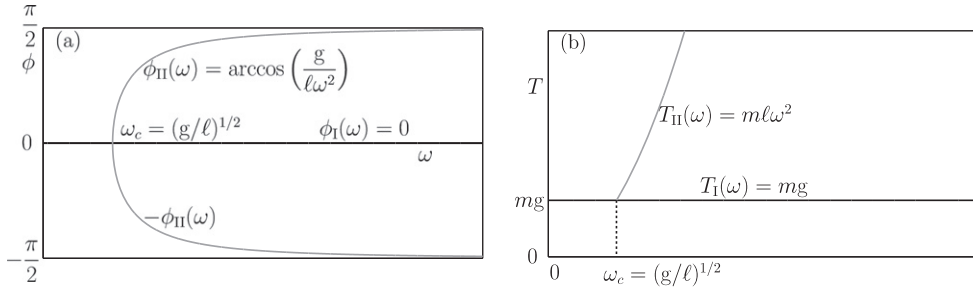


Figure 2. Families of equilibrium solutions for the rotating pendulum. (a) ϕ as a function of ω . (b) T as a function of ω .

condition (2). A straightforward calculation leads to the Jacobian of the system (4):

$$DF = \begin{pmatrix} \partial_T F_1 & \partial_\phi F_1 \\ \partial_T F_2 & \partial_\phi F_2 \end{pmatrix} = \begin{pmatrix} \cos \phi & -T \sin \phi \\ \sin \phi & (T - m\ell\omega^2) \cos \phi \end{pmatrix}, \quad (5)$$

with determinant

$$|DF(T, \phi, \omega)| = T - m\ell\omega^2 \cos^2 \phi.$$

Along branch I, this determinant adopts the value

$$|DF|_I \equiv |DF(T_I, \phi_I, \omega)| = m(g - \ell\omega^2), \quad (6)$$

whereas along branch II

$$|DF|_{II} \equiv |DF(T_{II}, \phi_{II}, \omega)| = m\ell\omega^2 \left(1 - \frac{g^2}{\ell^2\omega^4} \right). \quad (7)$$

For $\omega = \omega_c = (g/\ell)^{1/2}$, $|DF|_I = |DF|_{II} = 0$, and the uniqueness of solutions in a neighbourhood of that critical frequency is lost, as expected. The critical frequency, ω_c , is the only root for both determinants, and therefore both branches are locally unique for all $\omega > \omega_c$, so no new solutions are expected to be born from them.

2.2. Newton's method and numerical continuation

Typically, for an arbitrary value of the parameter $\alpha = \alpha^0$, the possible solution(s) or state(s), \mathbf{x}^0 , of system (1) are unknown. In general, system (1) for the n -unknowns, x_1, x_2, \dots, x_n , must be solved numerically for $\alpha = \alpha^0$ by means of a suitable algorithm such as the *Newton-Raphson* method [8], given by the iterative formula

$$\mathbf{x}^{(k+1)} = \mathbf{x}^{(k)} - \left(D\mathbf{F}_0^{(k)} \right)^{-1} \mathbf{F}_0^{(k)}, \quad k = 0, 1, 2, \dots, \quad (8)$$

where $\mathbf{x}^{(k)} = (x_1^{(k)}, x_2^{(k)}, \dots, x_n^{(k)})$ is the k th iterate of the method, $\mathbf{F}_0^{(k)} = \mathbf{F}(\mathbf{x}^{(k)}, \alpha^0)$, and $(D\mathbf{F}_0^{(k)})^{-1}$ stands for the inverse of the Jacobian matrix, $(D\mathbf{F}_0)_{ij} = \partial_{x_j} F_i(\mathbf{x}, \alpha^0)$, evaluated at $\mathbf{x} = \mathbf{x}^{(k)}$. In practice, many software packages allow the user to provide the Jacobian analytically. If that option is not available, the numerical package approximates the Jacobian via finite differences. The codes developed for this work make use of a second-order centred finite difference approximation, given by the expression

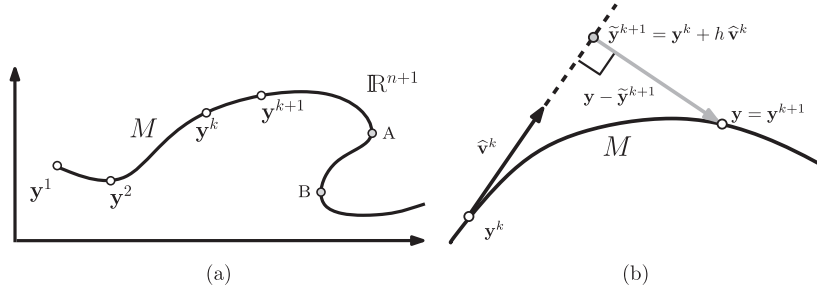


Figure 3. (a) Two-dimensional projection of a generic manifold, $M \subset \mathbb{R}^{n+1}$, implicitly defined by system (10). (b) Geometrical representation of the PAC algorithm: tangent predictor, $\tilde{\mathbf{y}}^{k+1}$, and normal corrector solution, \mathbf{y}^{k+1} , of the auxiliar appended system (14).

$$\partial_{x_j} F_i|_{\mathbf{x}} \approx \left[F_i(\mathbf{x} + h\mathbf{e}_j) - F_i(\mathbf{x} - h\mathbf{e}_j) \right] / (2h), \quad (9)$$

where \mathbf{e}_j is the j th canonical vector and $h \approx 10^{-8}$ in double-precision arithmetic [8]. This formula provides a truncation error of order $O(h^2)$.

The iteration must be started from an initial guess, $\mathbf{x}^{(0)}$, which should be close to the solution we seek, \mathbf{x}^0 , in order to have convergence (i.e., $\lim_{k \rightarrow \infty} \mathbf{x}^{(k)} = \mathbf{x}^0$). In that case, the method converges quadratically⁴ (i.e., $\|\mathbf{x}^{(k+1)} - \mathbf{x}^{(k)}\| < K \|\mathbf{x}^{(k)} - \mathbf{x}^{(k-1)}\|^2$), for some positive constant, K . Choosing random initial guesses may lead to nonconvergent iterations or, in some cases, convergence to other solutions different from the state we seek, \mathbf{x}^0 .

The general purpose of continuation techniques is to provide reliable numerical methodologies to track the solutions of (1) when the parameter, α , is varied.

Here we outline one of the more frequently used continuation algorithms in nonlinear physics: the *pseudo-arclength continuation* (PAC) [1]. In what follows, we define the state vector, $\mathbf{y} = (y_1, \dots, y_n, y_{n+1}) \equiv (x_1, \dots, x_n, \alpha)$, replacing the original variables of the problem since, as we will see later, the natural continuation parameter α will not always be the right variable to track solutions. In that sense, it is better to think of all the variables as potential continuation parameters. Consider a solution branch manifold, M in \mathbb{R}^{n+1} , implicitly defined by the n -dimensional nonlinear system of equations

$$\begin{aligned} F_1(y_1, \dots, y_n, y_{n+1}) &= 0 \\ F_2(y_1, \dots, y_n, y_{n+1}) &= 0 \\ &\vdots \\ F_n(y_1, \dots, y_n, y_{n+1}) &= 0. \end{aligned} \quad (10)$$

The coordinates of M can be implicitly parametrized by means of an arc-parameter, s (i.e., $\mathbf{y} = \mathbf{y}(s)$). The PAC algorithm is designed to obtain a numerically accurate discrete set of points, $\{\mathbf{y}^1, \mathbf{y}^2, \dots, \mathbf{y}^k, \dots\} \approx \{\mathbf{y}(s_1), \mathbf{y}(s_2), \dots, \mathbf{y}(s_k), \dots\}$, along M by applying suitable predictor and corrector methods. Figure 3(a) shows a two-dimensional projection of a prototypical continuation manifold, $M \subset \mathbb{R}^{n+1}$. Assume that \mathbf{y}^k is known (i.e., for $k = 1$, for instance); this can be accomplished by using the previously described Newton method applied to system (10) for the particular value of the parameter, $\alpha^1 = y_{n+1}^1$. The predictor stage provides a first approximation, $\tilde{\mathbf{y}}^{k+1}$, along the tangent direction of M at \mathbf{y}^k , dictated by

⁴ $\|\cdot\|$ stands for the standard Euclidean 2-norm in \mathbb{R}^n .

the unitary tangent vector, $\hat{\mathbf{v}}^k$ (see figure 3(b)). At any arbitrary point $\mathbf{y}(s) \in M$, this vector can be computed by implicit differentiation of system (10) with respect to the arc-parameter s , leading to the *homogeneous overdetermined* system of equations

$$\begin{bmatrix} \partial_{y_1} F_1 & \cdots & \partial_{y_{n+1}} F_1 \\ \partial_{y_1} F_2 & \cdots & \partial_{y_{n+1}} F_2 \\ \vdots & & \vdots \\ \partial_{y_1} F_n & \cdots & \partial_{y_{n+1}} F_n \end{bmatrix} \begin{bmatrix} v_1 \\ \vdots \\ v_n \\ v_{n+1} \end{bmatrix} = \begin{bmatrix} 0 \\ 0 \\ \vdots \\ 0 \end{bmatrix}, \quad (11)$$

where $v_j = \frac{d}{ds} y_j$ are the $n + 1$ components of the vector, $\mathbf{v} = (v_1, \dots, v_n, v_{n+1})$, tangent to the manifold, M , at $\mathbf{y}(s)$. System (11) contains n equations involving the $n + 1$ unknown components of \mathbf{v} . Since the tangent vector is undetermined up to an arbitrary multiplicative constant, this degeneracy can be eliminated by fixing one of the components of \mathbf{v} . The usual practice is to set $v_{i_0} = 1$ by introducing the solution vector, $\mathbf{v} = (v_1, \dots, v_{i_0-1}, 1, v_{i_0+1}, \dots, v_{n+1})$, so equation (11) now reads

$$\begin{bmatrix} \partial_{y_1} F_1 & \cdots & \partial_{y_{i_0-1}} F_1 & \partial_{y_{i_0+1}} F_1 & \cdots & \partial_{y_{n+1}} F_1 \\ \partial_{y_1} F_2 & \cdots & \partial_{y_{i_0-1}} F_2 & \partial_{y_{i_0+1}} F_2 & \cdots & \partial_{y_{n+1}} F_2 \\ \vdots & & \vdots & \vdots & & \vdots \\ \partial_{y_1} F_n & \cdots & \partial_{y_{i_0-1}} F_n & \partial_{y_{i_0+1}} F_n & \cdots & \partial_{y_{n+1}} F_n \end{bmatrix} \begin{bmatrix} v_1 \\ \vdots \\ v_{i_0-1} \\ v_{i_0+1} \\ \vdots \\ v_{n+1} \end{bmatrix} = - \begin{bmatrix} \partial_{y_{i_0}} F_1 \\ \partial_{y_{i_0}} F_2 \\ \vdots \\ \partial_{y_{i_0}} F_n \end{bmatrix}. \quad (12)$$

The i_0 th component must be chosen such that the resulting matrix appearing in (12) is nonsingular and well conditioned in order to ensure the uniqueness of solutions and the numerical stability of the algorithm. This requirement is crucial to avoid the failure of the continuation, particularly when the current estimate, \mathbf{y} , approaches a bifurcation point. Numerical continuation software packages [9] deal with this problem by computing the tangent directions of the bifurcating branches. In the present work, we simply avoid these pathological points by starting our continuation algorithm slightly away from the bifurcations.

The *tangent predictor*, $\tilde{\mathbf{y}}^{k+1}$, for the next point, \mathbf{y}^{k+1} , is obtained by locally approximating M along its tangent direction

$$\tilde{\mathbf{y}}^{k+1} = \mathbf{y}^k + h \hat{\mathbf{v}}^k, \quad (13)$$

where h is a suitably small step size (see figure 3(b)) and $\hat{\mathbf{v}}^k$ is the normalized vector that results from solving (12). The last stage of the PAC consists of the *correction*. Here we proceed with the simplest version based on solving the auxiliar or appended nonlinear system for the unknown, $\mathbf{y} \equiv \mathbf{y}^{k+1}$

$$\begin{bmatrix} F_1(\mathbf{y}) \\ F_2(\mathbf{y}) \\ \vdots \\ F_n(\mathbf{y}) \\ \langle \hat{\mathbf{v}}^k, \mathbf{y} - \tilde{\mathbf{y}}^{k+1} \rangle \end{bmatrix} = \begin{bmatrix} 0 \\ 0 \\ \vdots \\ 0 \\ 0 \end{bmatrix}. \quad (14)$$

This $(n + 1)$ -dimensional nonlinear system is solved with Newton's method, using $\mathbf{y}^{(0)} = \tilde{\mathbf{y}}^{k+1}$ as an initial guess. Geometrically, solving system (14) is equivalent to finding $\mathbf{y} \in M$ with $\mathbf{y} - \tilde{\mathbf{y}}^{k+1}$ orthogonal to the tangent prediction direction (see figure 3(b)).

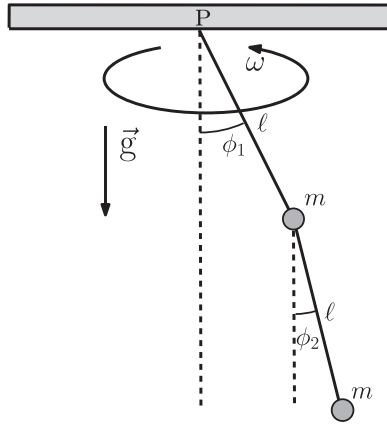


Figure 4. Double rotating pendulum.

In this work, we provide simple continuation MATLAB codes that deal with two particular problems in mechanics and thermodynamics. A complete description of the codes (`main.m`, `continuation.m`, `examplefun.m`, and `graphgenerator.m`) is provided in appendix A. These codes are only intended to illustrate the continuation techniques introduced here, not to serve as multipurpose tools for other applications. There are many continuation algorithms currently available; the state-of-the-art continuation algorithm is probably the MATCONT [9]⁵ package developed by Govaerts and Kuznetsov. This package embraces robust algorithms with many features such as step-size control of h (to avoid extremely small steps and to efficiently deal with turning or saddle-node points). It can also identify the branching points and tangent directions of new families of solutions emerging from them.

3. Numerical continuation in mechanics

In this section, we illustrate a first application of the numerical continuation algorithm to a slightly more complicated problem consisting of a double pendulum with two small spheres of mass m , connected by massless rigid rods of equal length, ℓ (see figure 4). As before, the system is forced to rotate with a constant angular speed, ω , around the vertical axis. As in the previous section, we are asked for equilibrium solutions in a ω -speed corotating frame. Let T_1 and T_2 be the tensions of the upper and lower rod, respectively. Application of Newton's laws for equilibrium leads to

$$T_1 \sin \phi_1 - T_2 \sin \phi_2 = m\omega^2 \ell \sin \phi_1, \quad (15a)$$

$$T_1 \cos \phi_1 - T_2 \cos \phi_2 = m g, \quad (15b)$$

$$T_2 \sin \phi_2 = m\omega^2 \ell (\sin \phi_1 + \sin \phi_2), \quad (15c)$$

$$T_2 \cos \phi_2 = m g. \quad (15d)$$

Formal substitution of (15c) and (15d) in (15a) and (15b), respectively, leads to the elimination of T_2 from the first two equations:

⁵ MATCONT project website, <http://sourceforge.net/projects/matcont/>.

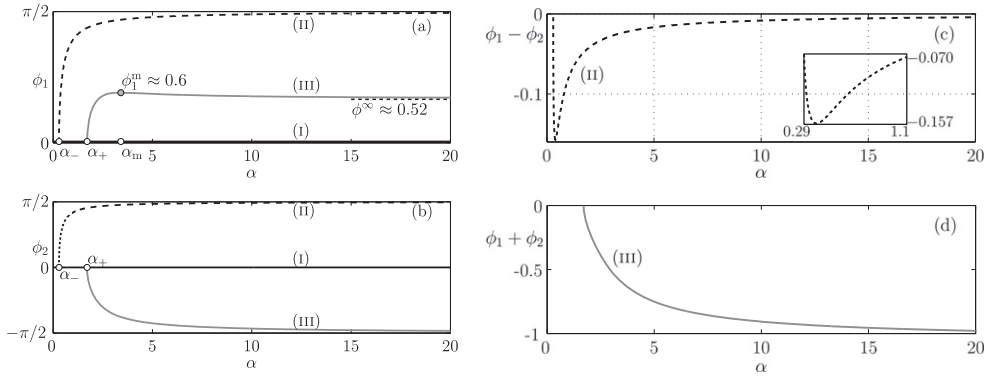


Figure 5. Families of equilibrium solutions for the double rotating pendulum. (a) ϕ_1 . (b) ϕ_2 . Their symmetric counterparts, $-\phi_1$ and $-\phi_2$, are not represented. (c) Difference $\phi_1 - \phi_2$ along BR-II; inset shows a detail of the minimum attained at $\alpha \approx 0.397$. (d) Sum of angles $\phi_1 + \phi_2$ along BR-III.

$$T_1 \sin \phi_1 = m\omega^2 \ell (2 \sin \phi_1 + \sin \phi_2), \quad (16a)$$

$$T_1 \cos \phi_1 = 2m g. \quad (16b)$$

For simplicity, we only seek equilibria within the domain

$$(\phi_1, \phi_2) \in [0, \pi/2) \times (-\pi/2, \pi/2),$$

bearing in mind that for each solution (ϕ_1, ϕ_2) there exists its symmetric version $(-\phi_1, -\phi_2)$. Quotients between equations (16a)–(16b) and (15c)–(15d) are used to eliminate the tensions from the original system, which is reduced to

$$\begin{aligned} F_1(\phi_1, \phi_2, \alpha) &= \tan(\phi_1) - \alpha(2 \sin \phi_1 + \sin \phi_2) = 0 \\ F_2(\phi_1, \phi_2, \alpha) &= \tan(\phi_2) - 2\alpha(\sin \phi_1 + \sin \phi_2) = 0, \end{aligned} \quad (17)$$

where $\alpha = \ell\omega^2/2g$ is a dimensionless parameter and the functions, $\tan(\phi_1)$ and $\tan(\phi_2)$, are well behaved within the search domain. We start by analysing the trivial solution branch, I: $(\phi_1, \phi_2) = (0, 0), \forall \alpha$. In this particular case, the Jacobian and its determinant can be calculated analytically, leading to $|DF|_I = 2\alpha^2 - 4\alpha + 1$. Since, in this case, the determinant is a quadratic polynomial, we expect at most two potential critical situations. This polynomial has roots at $\alpha_{\pm} = (2 \pm \sqrt{2})/2$, with $\alpha_- \approx 0.293$ and $\alpha_+ \approx 1.707$. At $\alpha = \alpha_-$, branch II (BR-II) is born (dashed curves in figures 5(a) and (b)). The qualitative properties of BR-II are similar to those corresponding to the single rotating pendulum seen in section 2. Angles ϕ_1 and ϕ_2 are both positive and grow monotonically, eventually stagnating at the asymptotic values, $(\phi_1, \phi_2) \rightarrow (\pi/2, \pi/2)$. However, angles ϕ_1 and ϕ_2 are different along BR-II, as shown in figure 5(c), where the difference, $\phi_1 - \phi_2$, is plotted as a function of α . For very small values of α , the difference, $\phi_1 - \phi_2$, is remarkable, with a maximum difference, $|\phi_1 - \phi_2|_{\max} \approx 0.157$, attained at $\alpha \approx 0.397$ (see inset in figure 5(c)). This discrepancy decreases for higher values of α , and is almost indistinguishable to the naked eye for a moderate value of $\alpha = 2$, as shown in figure 6(a). At $\alpha = \alpha_+$, an unexpected new family (BR-III) of solutions emerges from BR-I with $\phi_1 > 0$ and $\phi_2 < 0$. Along BR-III, ϕ_1 exhibits a rapid growth that attains a maximum value, $\phi_1^m \approx 0.6$, at $\alpha_m \approx 3.41$, denoted by

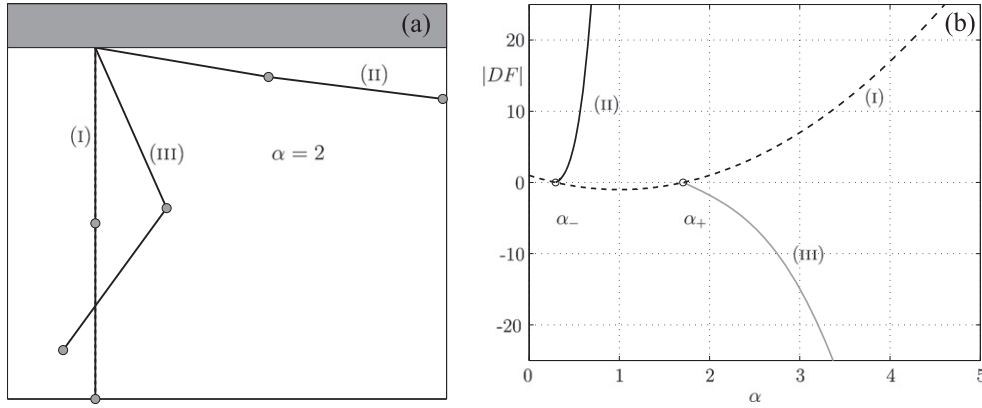


Figure 6. (a) Geometrical representation of the three possible equilibrium configurations for $\alpha = 2$. (b) Determinant of the Jacobian of system (17), evaluated along branches BR-I, BR-II, and BR-III. The values α_- and α_+ make the determinant zero.

the grey circle in figure 5(b). For $\alpha > \alpha_m$, this first angle slowly decreases and approaches an asymptotic value, $\phi^\infty \approx 0.52$. By contrast, the behaviour of ϕ_2 along BR-III is quite regular and similar, in absolute value, to that observed for ϕ_1 or ϕ_2 in BR-II, approaching an asymptotic value, $\phi_2 \rightarrow -\pi/2$. Along BR-III, angles ϕ_1 and ϕ_2 are not symmetrical ($\phi_2 \neq -\phi_1$), as can be seen in figure 5(d) where the quantity, $\phi_1 + \phi_2$, is plotted as a function of α .

Monitoring the Jacobian of BR-I is crucial for forecasting these new emerging branches, which can be continued by means of sophisticated strategies [9]. In the absence of such techniques, we simply explore the presence of new solutions by inspection (i.e., using Newton's method for $\alpha_- < \alpha < \alpha_+$ or $\alpha > \alpha_+$ to detect BR-II or BR-III, respectively, starting the iteration from different initial guesses until a new solution branch is identified). The Jacobian determinant of system (17) has been computed numerically along BR-I, BR-II, and BR-III, as seen in figure 6(b). Along branch BR-I, this determinant becomes zero at $\alpha = \alpha_+$ and $\alpha = \alpha_-$. According to the IFT, the uniqueness of implicit functions must be lost in a neighbourhood of α_+ and α_- . It is precisely at those roots where the Jacobian determinant, evaluated at the two other branches BR-II and BR-III, also vanishes. Away from these two singularities, α_- or α_+ , the determinants $|DF|_{II}$ and $|DF|_{III}$ were always found to be nonzero, thus indicating that both branches do not generate new families of solutions, at least within the range explored, $\alpha \in [0, 20]$.

Overall, the families of equilibrium solutions that we have just found constitute the scaffolding that would be crucial if we attempted to understand the dynamical counterpart of the problem. If the double rotating pendulums were allowed to oscillate, these branches of solutions would condition which configuration will be stable or unstable, and whether chaotic dynamics are present. However, a dynamical approach to the problem is far from the scope of this study.

4. Applications to phase transitions in thermodynamics

Another application of numerical continuation arises in the study of the phase transitions of real gases from the point of view of equilibrium thermodynamics. Isothermal compression of

a gas may lead to a liquid–vapour phase transition below a critical temperature, along which the pressure remains constant. Many academic courses and textbooks on thermodynamics address the theoretical study of this phenomena by means of the *van der Waals* equation. However, a similar analysis for the *Dieterici* equation is hard to find. These aforementioned equations qualitatively describe the shape of the isotherms of a real gas, and both may describe, to some extent, first-order phase transitions.

These equations are specific cases of a more general situation. Consider a gas obeying the equation of state

$$p = p(v, T), \quad (18)$$

where p is the pressure, v is the molar volume, and T is the temperature. The mathematical formulation will henceforth be established in *reduced* thermodynamic variables so that the coordinates of the *critical point* [10] satisfying

$$\partial_v p = \partial_v^2 p = 0, \quad (19)$$

are

$$p_c = v_c = T_c = 1.$$

Figure 7 shows three generic supercritical, critical, and subcritical isotherms with $T > T_c$, $T = T_c$, and $T < T_c$ in equation (18), respectively. Computing the volumes, v_ℓ and v_g , for an arbitrary subcritical isotherm, $T < T_c = 1$, is a challenging problem. These volumes are obtained by imposing two conditions. The first condition is usually called the *lever rule* (i.e., the shadowed areas of regions I and II in figure 7 must be equal). For a detailed derivation of this rule, refer to section 3.4 of Callen's monograph on thermodynamics [10]. The second constraint is that the pressures, $p_\ell = p(v_\ell, T)$ and $p_g = p(v_g, T)$, must coincide (see figure 7). The two aforementioned conditions lead to the system of equations to be solved:

$$\begin{aligned} F_1(v_\ell, v_g, T) &= \int_{v_\ell}^{v_g} p(v, T) dv - (v_g - v_\ell)p(v_\ell, T) = 0 \\ F_2(v_\ell, v_g, T) &= p(v_g, T) - p(v_\ell, T) = 0. \end{aligned} \quad (20)$$

In this case, the Jacobian matrix of system (20) is

$$DF = \begin{pmatrix} \partial_{v_\ell} F_1 & \partial_{v_g} F_1 \\ \partial_{v_\ell} F_2 & \partial_{v_g} F_2 \end{pmatrix} = \begin{pmatrix} (v_\ell - v_g)\partial_v p(v_\ell, T) & p(v_g, T) - p(v_\ell, T) \\ -\partial_v p(v_\ell, T) & \partial_v p(v_g, T) \end{pmatrix}. \quad (21)$$

System (20) admits the trivial solution, $v_\ell = v_g$, along which the Jacobian matrix (21) is rank-deficient with $\text{rank}(DF)_{v_\ell=v_g} = 1$, and is therefore singular. According to the IFT, the uniqueness of solutions may be lost along that trivial branch. However, the physically meaningful solution branch is born precisely at the critical point, $(v_\ell, v_g) = (1, 1)$, where the Jacobian matrix is identically zero (i.e., $\partial_v p(1, T) = 0$). The continuation algorithm will successfully identify the physically meaningful branch we seek if it is started locally near that critical point. This situation is illustrated in figure 8 for the van der Waals gas, to be studied in detail in the next section.

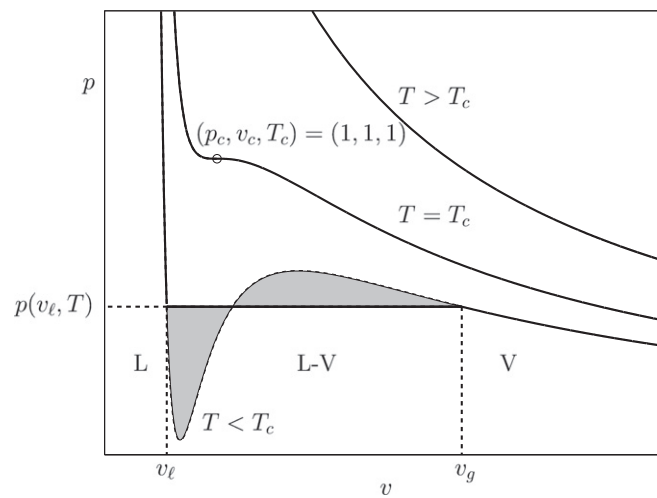


Figure 7. Lever rule across a generic subcritical isotherm indicating liquid (L), liquid–vapour (L–V), and vapour (V) regions. The white circle is located at the critical point, and the pressure at v_g must be $p(v_\ell, T)$.

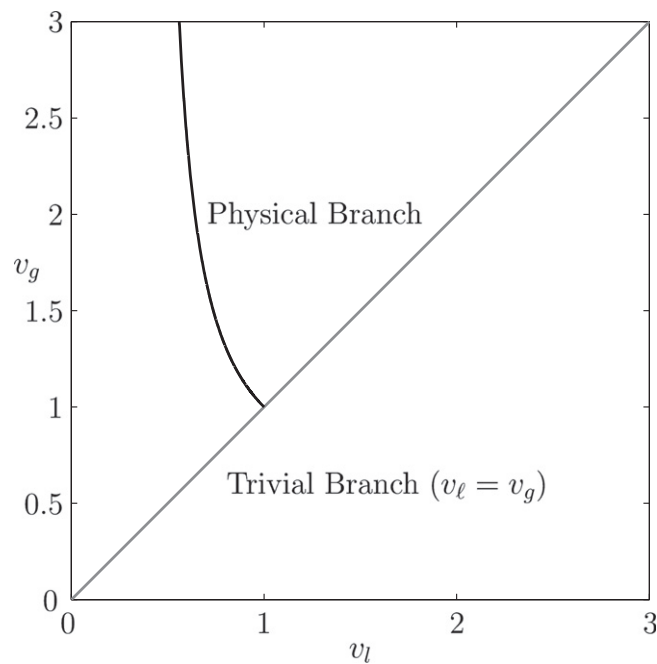


Figure 8. Physical solution branch (black) emerging from the critical point, ($v_\ell = v_g = 1$).

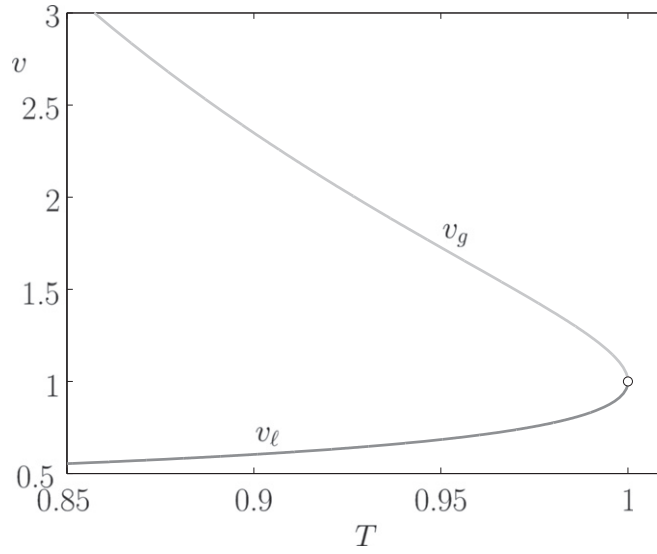


Figure 9. Two-dimensional projection of coexistence curves, v_ℓ (dark grey) and v_g (light grey), as a function of T resulting from the continuation algorithm.

4.1. van der Waals equation

The previous discussion can be applied to the reduced van der Waals equation [11],

$$p(v, T) = \frac{8T}{3v-1} - \frac{3}{v^2}, \quad (22)$$

defined for $v > \frac{1}{3}$ and $T > \frac{27}{32}$. In this particular case, the isothermal integration appearing in (20) can be evaluated analytically so that the system can be expressed explicitly in terms of v_ℓ and v_g :

$$F_1(v_\ell, v_g, T) = \log\left(\frac{3v_g-1}{3v_\ell-1}\right) + \frac{9}{4T}\left(\frac{1}{v_g} - \frac{1}{v_\ell}\right) - \frac{1}{3v_g-1} + \frac{1}{3v_\ell-1} = 0$$

$$F_2(v_\ell, v_g, T) = \frac{8T}{3}\left(\frac{1}{3v_g-1} - \frac{1}{3v_\ell-1}\right) - \frac{1}{v_g^2} + \frac{1}{v_\ell^2} = 0. \quad (23)$$

Figure 9 shows a two-dimensional projection of the coexistence curves, $v_\ell(T)$ and $v_g(T)$, resulting from the continuation algorithm applied to system (23) starting near the critical point, $(v_\ell, v_g, T) = (1, 1, 1)$, using Newton's method. In this case, both curves are born at the tangent or saddle-node point [1], $T = v = 1$. To avoid convergence to the $v_\ell = v_g$ unphysical solution, the continuation algorithm must be started slightly away from the critical point, ($T < 1$), using different values of v_ℓ and v_g as initial guesses satisfying $v_\ell < 1 < v_g$. Figure 10(a) shows the two-dimensional p - v diagram, including the solution curves previously shown in figure 9. Figure 10(b) shows a three-dimensional projection of the van der Waals surface, along which the coexistence phase region has been shadowed. Finally, table 1 contains the coordinates of the coexistence boundaries within the temperature range, $T \in [0.85, 1.00]$. The numerical values reported in table 1 have been provided with at least 12 significant figures.

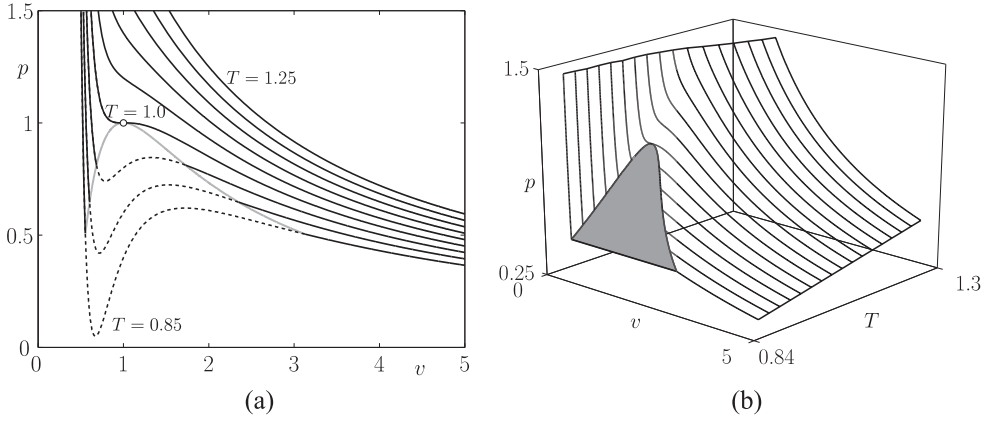


Figure 10. (a) Isotherms from van der Waals equation within allowed ranges of temperature. Portions of the isotherms within the interval (v_ℓ, v_g) have been depicted with dashed curves. (b) Three-dimensional representation of the $p(v, T)$ surface, excluding the transition region (shaded).

Table 1. Numerical values of coexistence boundaries for the van der Waals gas.

T	v_ℓ	v_g	p
1.000	1.000 000 000 000	1.000 000 000 000	1.000 000 000 000
0.975	0.755 140 600 754	1.436 931 258 000	0.902 985 170 975
0.950	0.684 122 113 656	1.727 071 192 256	0.811 879 243 364
0.925	0.637 851 638 159	2.024 621 393 007	0.726 585 053 520
0.900	0.603 401 903 178	2.348 842 376 202	0.646 998 351 872
0.875	0.576 016 046 000	2.712 408 236 896	0.573 007 253 114
0.850	0.553 360 458 440	3.127 639 292 441	0.504 491 649 787

4.2. Dieterici equation

The Dieterici equation state in reduced thermodynamic coordinates is [11]:

$$p(v, T) = \frac{T}{2v-1} \exp\left(2 - \frac{2}{vT}\right), \quad (24)$$

with $v > \frac{1}{2}$ due to the finite size of the molecules (similar to the restriction $v > \frac{1}{3}$ in the van der Waals equation). In this case, the integral appearing in F_1 of system (20) cannot be evaluated analytically and must be computed numerically by means of a quadrature formula. In this case, the system of equation (20) is

$$\begin{aligned} F_1(v_\ell, v_g, T) &= I_N(v_\ell, v_g, T) - (v_g - v_\ell)p(v_\ell, T) = 0 \\ F_2(v_\ell, v_g, T) &= \frac{1}{2v_g - 1} \exp\left(2 - \frac{2}{v_g T}\right) - \frac{1}{2v_\ell - 1} \exp\left(2 - \frac{2}{v_\ell T}\right) = 0, \end{aligned} \quad (25)$$

where $I_N(v_\ell, v_g, T)$ stands for the quadrature approximation of the isothermal integral based on $N + 1$ quadrature points, $\{v_0, v_1, \dots, v_N\}$:

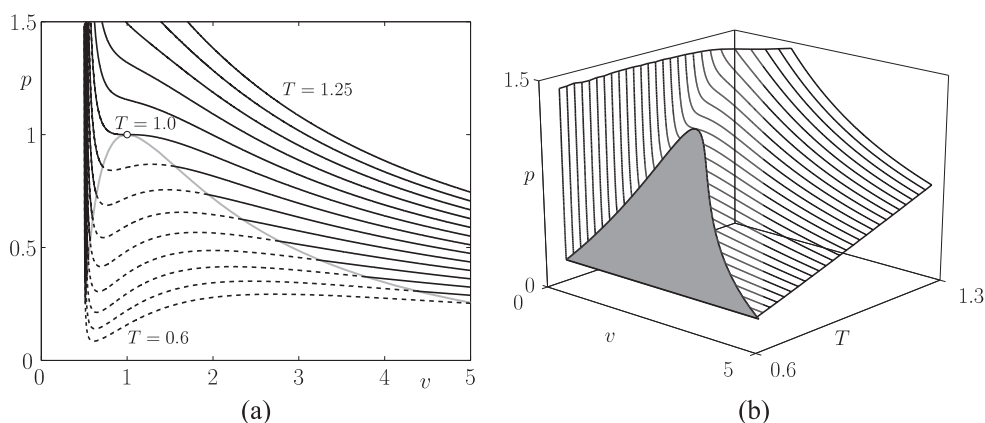


Figure 11. (a) Isotherms from Dieterici's equation. Portions of the isotherms within the interval (v_ℓ, v_g) have been depicted with dashed curves. (b) Three-dimensional representation of the $p(v, T)$ surface, excluding the transition region (shaded).

Table 2. Numerical values of coexistence boundaries for Dieterici's equation.

T	v_ℓ	v_g	p
1.000	1.000 000 000 000	1.000 000 000 000	1.000 000 000 000
0.975	0.781 111 623 679 646	1.352 987 818 610 43	0.927 216 952 746 984
0.950	0.716 033 340 120 983	1.560 710 036 604 51	0.858 736 883 359 602
0.925	0.673 844 398 915 984	1.754 631 313 647 76	0.794 366 307 368 327
0.900	0.642 840 743 502 614	1.947 036 581 542 20	0.733 915 739 055 988
0.875	0.618 652 754 731 553	2.142 917 821 446 63	0.677 199 845 628 736
0.850	0.599 112 607 104 091	2.345 112 466 346 68	0.624 037 602 449 63
0.825	0.582 971 832 431 844	2.555 593 223 081 45	0.574 252 449 749 519
0.800	0.569 440 426 495 074	2.775 938 477 766 09	0.527 672 451 399 130
0.775	0.557 984 544 445 464	3.007 546 876 738 02	0.484 130 456 505 169
0.750	0.548 225 305 970 880	3.251 754 373 220 76	0.443 464 264 767 860
0.725	0.539 883 215 514 119	3.509 910 262 471 75	0.405 516 796 684 844
0.700	0.532 745 387 783 188	3.783 436 314 821 55	0.370 136 269 772 613
0.675	0.526 645 096 620 475	4.073 881 129 546 49	0.337 176 381 952 146
0.650	0.521 448 402 472 000	4.382 977 027 299 68	0.306 496 503 042 278
0.625	0.517 045 052 448 858	4.712 704 912 470 43	0.277 961 874 833 345
0.600	0.513 342 069 858 104	5.065 372 031 097 48	0.251 443 819 363 877

$$I_N(v_\ell, v_g, T) = \sum_{j=0}^N w_j p(v_j, T), \quad (26)$$

with $\{w_0, w_1, w_2, \dots, w_N\}$ being the quadrature weights of the formula. Since our purpose is to have a highly accurate evaluation of F_1 , we have used the *Clenshaw–Curtis* quadrature formula [12]. This quadrature has recently been vindicated as a competitive alternative to classical Gauss formulas [13] since it also provides exponential convergence, but with the advantage that the nodes and weights of the corresponding formulas are known explicitly for

arbitrary N , and thus requiring much less computational cost overall. The coexistence boundaries resulting from the continuation are summarized in figure 11 and also in table 2 for $T \in [0.6, 1]$. The reported values in table 2 are accurate to 12 decimal places. For the moderate subcritical temperatures used, the number of quadrature nodes required to get the aforementioned accuracy is reasonably low to moderate, with N typically ranging from 26 to 200. However, for small values of T , the lower bound of integration, v_ℓ , approaches the singular value $1/2$, where Dieterici's equation fails to be defined, as seen in figure 11(a) or table 2. As the limit $T \rightarrow 0^+$ is approached, the integrand becomes singular at $v = v_\ell$, thus deteriorating the exponential convergence of the quadrature rule. Dealing with this numerical pathology is far beyond the scope of the present work.

5. Conclusion

This work illustrates how numerical continuation algorithms can be applied to solve parameter-dependent nonlinear physical equations arising in undergraduate mechanics or thermodynamics courses. The computational techniques required to solve the aforementioned problems include Newton's method and quadrature formulas for numerical integration. Documented MATLAB codes are included as supplementary material (see stacks.iop.org/ejp/36/015015/mmedia). These codes solve the mechanics and thermodynamics problems exemplified in this work, but they can be adapted to solve similar problems arising in other branches of undergraduate physics.

Appendix A. MATLAB codes

The aim of the codes is to provide the vapour–liquid transition curves for substances obeying van der Waals and Dieterici equations of state, as well as the equilibrium angles for the rotating double pendulum. For the thermodynamics problems, the codes provide numerical tables of the coexistence curves with at least 12 correct significant digits. The code is divided into different files that contain functions used by the main script:

- `main.m`: main script.
- `continuation.m`: continuation algorithm.
- `examplefun.m`: M-function to which the continuation is applied.
- `graphgenerator.m`: M-function that provides the figures.

To run the program, copy all the files in a directory and set this folder as MATLAB's working folder. Then type `main` in MATLAB's prompt. The `main` code makes use of the function `examplefun.m`, which adapts itself to the mechanical or thermodynamical cases by assigning the following values to the global variable, `flag`:

- `flag=1` : double pendulum.
- `flag=2` : van der Waals equation.
- `flag=3` : Dieterici equation.

1. `continuation.m`

This function performs the PAC of the function `fun` from the initial point `y0` and during `maxIt` iterations of step `h`. This function is invoked as follows:

```
yCont = continuation(fun, y0, h, tol, maxIt);
```

with input arguments:

- `fun`: corresponding to the system (10) satisfying $\text{fun}(y) = 0$.
- `y` = [$y_1 \dots y_n y_{n+1}$] : $n + 1$ variable array.
- `y0`: starting continuation point.
- `h`: step size.
- `tol`: tolerance of the Newton iteration.
- `maxIt`: total number of iterations.

The output arguments are:

- `yCont`: $(n+1) \times m$ matrix with $m = \text{MaxIt}$ containing:

$$yCont = \begin{bmatrix} y_1^1 & \dots & y_1^m \\ \vdots & & \vdots \\ y_n^1 & \dots & y_n^m \\ y_{n+1}^1 & \dots & y_{n+1}^m \end{bmatrix}.$$

Within `continuation.m`, two inner routines are used:

- `jac.m`: second-order finite difference approximation of the Jacobian of an arbitrary vector field $\mathbf{F}: \mathbb{R}^{n+1} \rightarrow \mathbb{R}^n$. The calling sequence is

$$jacF = jac(fun, y);$$

where `jacF` is the array containing the Jacobian-approximated matrix of function `fun` evaluated at `y`.

- `newtoncorrector.m`: correction to the predictor used in `continuation`. The calling sequence is:

$$corr = newtoncorrector(fun, pred, tanVec, tol);$$

where `fun` is the continuation function, `pred` is the current predictor, `tanVec` is the tangent vector to the curve at that point, and `tol` is the tolerance of the Newton iteration. The returning value is `corr` (i.e., next continued point).

2. `examplefun.m`

Evaluates the function to perform the continuation and the subroutine `weightCC`, which computes the Clenshaw–Curtis weights of integration (Dieterici's cases) in case `flag=3`. The calling sequence is:

$$fun = examplefun(y); .$$

The numerical value of `flag` must be assigned before invoking this function:

- `flag = 1`: the double pendulum approach is taken, and the components of the input variable `y` are $y(1) = \phi_1$, $y(2) = \phi_2$, and $y(3) = \alpha$. The components of `F` are those explained in this paper.
- `flag = 2`: the van der Waals equation is applied. In this case, the components of `y` are $y(1) = v_l$, $y(2) = v_g$, and $y(3) = T$.
- `flag = 3`: the Dieterici equation of state is used and no analytic integration can be done. In this case, `weightCC` is used to provide the Clenshaw–Curtis quadrature weights. This subroutine is invoked as follows:

$$weights = weightCC(N);$$

this function computes $N + 1$ Clenshaw–Curtis quadrature weights, and stores them in the global variable, `weights`.

3. `graphgenerator.m`

The function generates three figures:

- ϕ_1 as a function of α .
- ϕ_2 as a function of α .
- Two graphics of the isotherms and the coexistence region, for van der Waals and Dieterici, and two tables with the values of T , v_l , v_g , and p .

The function has no output arguments, and is called

```
graphgenerator(yContII, yContIII, plotVdw,
              tableVdw, plotD, tableD);
```

where all the input arguments contain the necessary information to generate the figures.

References

- [1] Kuznetsov Y A 2004 *Elements of Applied Bifurcation Theory* 3rd edn (New York: Springer)
- [2] Motter A E and Campbell D K 2013 Chaos at fifty *Phys. Today* **66** 27–33
- [3] Shinbrot T, Grebogi C, Wisdom J and Yorke J A 1992 Chaos in a double pendulum *Am. J. Phys.* **60** 491
- [4] Levien R B and Tan S M 1993 Double pendulum: an experiment in chaos *Am. J. Phys.* **61** 1038
- [5] Groff J R 2013 Exploring dynamical systems and chaos using the logistic map model of population change *Am. J. Phys.* **81** 725
- [6] Iooss G and Joseph D D 1997 *Elementary Stability and Bifurcation Theory* 2nd edn (New York: Springer)
- [7] Marsden J E and Hoffman M J 1993 *Elementary Classical Analysis* 2nd edn (New York: Freeman)
- [8] Kincaid D and Cheney W 2002 *Numerical Analysis—Mathematics of Scientific Computing* 3rd edn (Pacific Grove: Brooks/Cole)
- [9] Dhooge A, Govaerts W and Kuznetsov Yu A 2003 *ACM TOMS* **29** 141
- [10] Callen H B 1985 *Thermodynamics and an Introduction to Thermostatistics* 2nd edn (New York: Wiley)
- [11] Sadus R J 2001 *J. Chem. Phys.* **115** 1460
- [12] Davis P J and Rabinowitz P 1984 *Methods of Numerical Integration* 2nd edn (London: Academic)
- [13] Trefethen L N 2008 Is Gauss quadrature better than Clenshaw–Curtis? *SIAM Rev.* **50** 67